

*J. Synchrotron Rad.* (1999). 6, 244–246

## Numerical determination of a true absorption spectrum from grazing-incidence fluorescence EXAFS data

J.M. Lee,<sup>a</sup> Heui-Han Yoo<sup>a</sup> and Minsoo Joo<sup>b</sup>

<sup>a</sup>Beamline Research Division, Pohang Accelerator Laboratory, POSTECH, Pohang, 790-784, Korea; <sup>b</sup>Korea Electric Power Research Institute, Taejeon 305-380, Korea; jaymin@postech.ac.kr,

The fluorescence EXAFS spectra, measured at a grazing incidence angle larger than the critical angle for total reflection, were examined to test a numerical conversion from the distorted fluorescence data to the 'true' absorption spectra, achieving a reliable transferability between the transmission and the fluorescence data. Under various entrance and exit angles, full numerical corrections were made in terms of the sample's self-absorption, the measurement geometry, and the energy dependent efficiency function of the  $I_0$  ionization chamber detector. Particularly, a numerical code was developed for the x-ray fluorescence geometry configured without a scattering discrimination filter. For an illustration of glancing-angle fluorescence EXAFS spectra, we performed an in-situ measurement for the thick porous nickel specimens undergoing a heated-air surface oxidation process.

**Keywords:** Grazing Incidence; Fluorescence EXAFS; Numerical Code.

### 1. Introduction

Unlike the conventional transmission EXAFS data, the fluorescence spectra are largely distorted and dependent on the entrance and the exit angles of geometrical probing. The unfiltered  $I_F/I_0$  spectra involved with amount of scattered background represent a severe distortion of the edge shape and a measurable suppression of the EXAFS amplitude. Such signal deformation problem was pointed out as systematic errors in fluorescence EXAFS, involving the self-absorption and the depth effect. (Bunker, 1988) Although studies were motivated to search the optimum experimental setup by simulating numerical correction of the fluorescence distortions (Troger *et al.*, 1992; Brewe *et al.* 1994), any reliable numerical recipe is not widely spread in use.

Regardless of such handicap of data analysis, fluorescence EXAFS technique is so far referred to an appropriate detection mode of x-ray for the diluted specimens. Recently, many studies of chemical and structural probes for the thin film deposited specimens still inquire the merit of fluorescence EXAFS technique using GIX (Grazing Incidence X-ray) or glancing-angle geometry (Oyanagi, 1998). For the thin film of the thickness less than one penetration depth, the small grazing incidence angle geometry is more appropriate. For instance, the entrance angle of 3-5 degrees can make the information depth extended up to 10-20 times. The grazing-incidence angles in this range are much larger than the critical angle for total reflection, and the fluorescence plus scattering signals will be detected largely compared to the reflection signal.

### 2. Description of Fluorescence EXAFS Signal

In the fluorescence EXAFS mode, the flux of incident x-ray at the monochromatic energy ( $E_i$ ) is monitored by the front semitransparent ionization chamber ( $I_0$ ), and a combination of fluorescence photon energy ( $E_F$ ) and the scattered radiation ( $E_F < E_{sc} < E_i$ ) are measured by the rear fluorescence detector ( $I_F$ ). The scattered radiation can be largely removed by a combination of Z-1 filter and slit mask, as normally employed in the Lytle detector. (Stern *et al.*, 1979; Lytle *et al.*, 1984). In an advanced technique, a suitable energy dispersive detector (such as Si/Li) can discriminate the background signal caused by scattering.

The non-zero background is present when the fluorescence signal is detected without a scattering discrimination filter. As pointed out in other study (Troger *et al.*, 1992), the  $I_F/I_0$  spectra, modeled under a self-absorption geometry for a thick sample, can

$$J(E_i) = I_F(E_F) / I_0(E_i) \\ = \frac{\mu_f(E_i)}{\mu_T(E_i) + \mu_T(E_F) \sin(\theta) / \sin(\phi)} + J_{back}(E_i)$$

be expressed as:

**Eq(1)**

Here,  $\theta$  is the entrance graze angle of the incident x-rays, and  $\phi$  is the exit graze angle of the detected fluorescence radiation with respect to the sample surface. In this equation,  $\mu_T(E_i)$  is the sample's self absorption (i.e. the total absorption coefficient at energy  $E_i$ ), and  $\mu_f(E_i)$  is fluoresced portion from the particular element of interest, that is a part of  $\mu_T(E_i)$ . On the other hand,  $J_{back}(E_i)$  is attributed to the scattered background signal altered by detector's sensitivity and the energy dependence of absorption along the beam path between two detectors.

### 3. Numerical Determination of True Absorption Spectrum

At the starting point of numerical procedure, it is better to generate the corrected spectrum,  $j_K(x) = J(x) K_D(x) K_S(x)$ , by introducing a coordinate transformation of  $x = (E_i - E_0) / (E_0 - E_F)$  for the threshold energy ( $E_0$ ). Here, energy correction functions,  $K_D(x)$  and  $K_S(x)$ , are dependent on the detector sensitivity and the scattering geometry, respectively. In a real situation,  $K_S(x)$  is less significant, but  $K_D(x)$  is a considerable energy dependent function of  $I_0$ -detector sensitivity.

For a functional simplification, the nominal absorption spectrum is defined as  $\alpha(x) = \mu_T(x) / \mu_T(-1)$ , and the  $j_K(x)$  spectrum is normalized to  $j(x)$  by the proportional constant ( $W_0$ ) which is the amplitude gain associated with the detector's sensitivity. (The examples for  $j(x)$  and  $\alpha(x)$  are displayed in figure 1, but the relevant details will be discussed later.)

By defining a geometrical factor as  $g_0 = \sin(\theta) / \sin(\phi)$ , eq(1) can be transformed to the final expression for  $j(x)$  as:

$$j(x) = j_K(x) / W_0 \\ = \frac{\alpha(x)}{\alpha(x) + g_0} + \left[ \frac{B_0}{\alpha(x) + g_0 \xi_0} - \frac{1}{\alpha(x) + g_0} \right] \alpha_0 H(x)$$

**Eq (2)**

where

$$B_0 = (1 + g_0 \xi_0 / \alpha_0) j(0) / W_0$$

**Eq(3)**

is a self-consistent parameter.

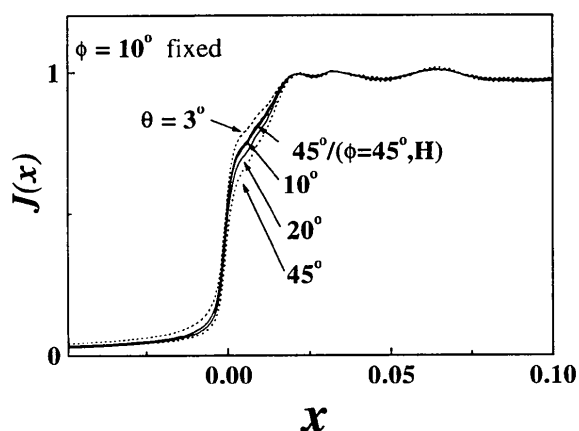


**Figure 1.** Normalized  $j(x)$  spectra at various incidence angle geometry. The observation angle ( $\phi$ ) is fixed at 10 degrees, and the grazing incidence angles ( $\theta$ ) are noted in figure. The case of the conventional fluorescence geometry using a horizontal right-angle geometry (i.e. the entrance and the exit angles,  $\theta$  and  $\phi$ , are 45 degrees) is shown for a comparison.

First, it is obvious that the first term of eq(2) represents the first term of eq(1). Second, the second term of eq(2) is corresponding to  $J_{back}(E_i)$  in eq(1), even though a physical meaning is not well specified yet. Basically,  $j(x)$  becomes a function of  $\alpha(x)$  and  $g_o$  parameter. Typically,  $\alpha_o$  is approaching to  $\alpha(0)$  along the pre-edge slope's extrapolation at the threshold energy  $E_o$  (i.e.  $x=0$ ). (Also,  $\alpha(-1)=1$  and  $0 < \alpha_o < 1$ ) To test the functional characteristics between  $j(x)$  and  $\alpha(x)$ , we treated  $\xi_o$  as a characteristic parameter ( $0 < \xi_o < 1$ ) and  $H(x)=(\alpha_o)^x$  as a monotonically decaying function, representing a specific scattered background part.

In this equation, the  $j(x)$  consists of the principal part (oscillating  $\alpha(x)$  dependence) plus the background part (non-oscillating  $\alpha_o H(x)$  dependence). In the principal part, when  $g_o$  becomes smaller, the desired term  $\alpha(x)$  in the numerator would

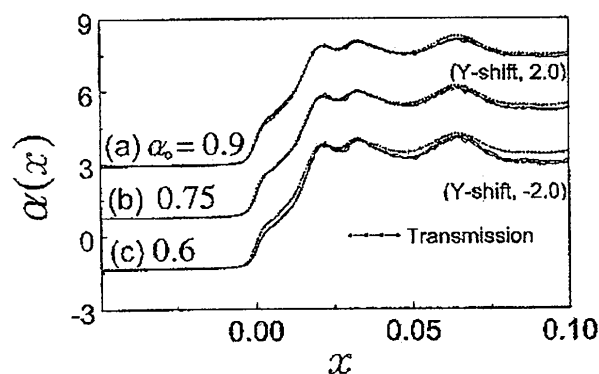


**Figure 2.** Fitting test of transferability between the transmission and fluorescence data, under the specific  $\alpha_o$  values of (a) 0.9 (b) 0.75 and (c) 0.6 assumed in the numerical conversion code. The  $\alpha(x)$ -spectra are numerically converted from the grazing angle fluorescence data. In this measurement, the observation angles ( $\phi=85^\circ, 60^\circ, 30^\circ$  and  $10^\circ$ ) are chosen at a fixed entrance graze angle,  $\theta=3^\circ$ .

be canceled out by the same term in the denominator; therefore the spectra features (e.g. EXAFS amplitudes) are strongly suppressed. Because both parts include the oscillating part  $\alpha(x)$  at each denominator, the fluorescent signal is affected by the correlation between the absorption spectrum  $\alpha(x)$  and the background part  $\alpha_o H(x)$ . At this point, one can know that no background-removal filtering is a better experimental setup for the glancing angle fluorescence measurements.

The material constants,  $\alpha(x)$  and  $\alpha_o$ , can be determined from the  $j(x)$  for a fixed  $g_o$  (the given geometrical parameter). The variable set for  $\alpha(x)$  can be expressed in a quadratic equation for that for  $j(x)$ . In the computation process, it is required to set an arbitrary  $W_o$  value beforehand. When both  $\alpha(x)$  and  $j(x)$  are known,  $W_o$  can be determined consequently. When  $W_o$  is ambiguous,  $\alpha(x)$  is not uniquely determined. Mathematically, however, it is possible to solve  $\alpha(x)$  and  $W_o$  simultaneously from the fluorescence data measured at two different  $g_o$  conditions.

#### 4. Empirical Results and Discussions

For this experiment at PLS 3C1 EXAFS beamline (Lee *et al*, 1998), the monochromatic beam was introduced to the entrance slit definition of 5mm horizontal and 0.5mm vertical width. The  $I_o$  gas ionization chamber was employed to measure the incident flux of x-ray photon, and the planar semiconductor detector to collect the fluorescence signal. Grazing incidence angle geometry was chosen using the rotary sample stage, and the exit

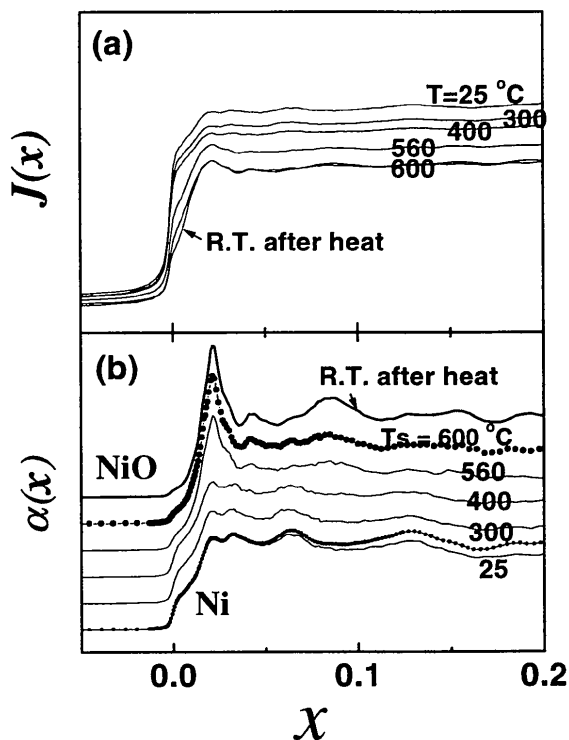


**Figure 3.** (a) The raw data of GIX fluorescence experiment for the porous nickel specimens during the oxidation process at the heating temperatures up to 600°C. (b) The true absorption spectra numerically converted from the distorted fluorescence data. The oxidation of Ni specimens is clearly observed with significant EXAFS modifications as if the transmission measurement of thin foil is made.

observation angles were adjusted by positioning the fluorescence detector. The distance from sample to fluorescence detector was 10cm, and the active area of fluorescence detector was configured in 30mm diameter. Fluorescence EXAFS spectra for Ni K-edge (8333eV) were measured from 1mm thick porous nickel specimen of the fuel cell electrode.

To evaluate  $j(x)$  in eq(2), we consider the fluorescence photon energy (7565eV) by taking a weighted average between K<sub>L</sub> and K<sub>LL</sub> lines. In figure 1, the normalized  $j(x)$  spectra are displayed at various grazing incidence angle geometry;  $\theta=3\sim 45$  degrees at a fixed observation angle ( $\phi=10$  degrees). The degrees of XANES signal distortion is associated with the selection of grazing incidence angle. Here the smaller graze angle is attributed to the larger signal deformation of edge shape. When we solve for  $\alpha(x)$  from  $j(x)$ , the quantitative values for  $\alpha_v$ (true absorption) and  $W_v$ (amplitude gain) is determined consequently. Our computation code is proved by a proper simulation that  $\alpha(x)$ -curves are coincident at any  $g_v$ -parameter when appropriate  $\alpha_v$  and  $W_v$  values are chosen. Our empirical analysis results that  $\alpha_v=0.75$  is proper at the minimum deviation (or maximum correlation) in  $\alpha(x)$  over the different measurement geometry. In this way, one can determine the true value of  $\alpha_v$ .

Figure 2 shows the absorption spectrum  $\alpha(x)$ , numerically converted from  $j(x)$ , at different measurement geometry in  $g_v=0.053\text{-}0.301$  for various observation angles at a fixed entrance graze angle,  $\theta=3^\circ$ . By assuming specific  $\alpha_v$  values as (a) 0.9 (b) 0.75 and (c) 0.6, we tested the validity of our numerical conversion code. When  $\alpha_v=0.75$  for the case of (b), we can obtain the best fit; significant coincidence in XANES and EXAFS region indicates the validity of the empirical transferability between the transmission and the fluorescence data. Therefore,  $\alpha_v=0.75$  becomes an appropriate solution for specifying the material constant,  $\alpha(x)$ .

The numerical conversion relationship, from  $j(x)$  to  $\alpha(x)$ , is now applied to probe the time-resolved changes of the in-situ sample at a measurement geometry fixed. By solving the coincidence condition of  $\alpha(x)$ -curves at two different detector observation angles ( $\phi$ ), 45 and 85 degrees, we first solved the appropriate  $\alpha_v$  and  $W_v$  values from the measured data at room temperature. A fixed grazing incidence angle of 5 degrees,  $\alpha_v=0.75$  and  $W_v=1.14$  was obtained. Then we applied these pre-determined parameters to the new data set at higher oxidation temperatures. These results of true absorption spectra are shown in figure 3.

To avoid the complexity in the surface oxidation depth profile, our experiment was performed on the thick porous nickel specimens of the fuel cell electrodes undergoing a heated-air surface oxidation. In our data, the uniform depth profile of oxidation can simplify our numerical treatment. The initial Ni phase at room temperature is changed to the NiO phase above 560°C of sample heating temperatures. Actually, we observed the quick oxidation process around 500°C, but that case is omitted in this figure. That feature is strongly distorted and suppressed consequently because the scattering background increases with a somewhat rapid oxidation process.

## 5. Conclusion

Distorted fluorescence XANES and suppressed EXAFS signals are numerically corrected to the true absorption coefficient, which is unique material constant compatible to that of transmission measurement. Through our numerical plus empirical test, for solving the proper choice of  $\alpha_v$  (the true absorption coefficient) and  $W_v$  (the measurement amplitude gain)

parameters, we verified both quantitative excellence and potential usefulness for the application of the grazing incidence x-ray fluorescence EXAFS measurement.

Experiments at PLS were supported in part by MOST and POSCO.

## Reference

- Brewe, D.L., Pease, D.M. & Budnick, J.I., Phys. Rev. B. (1994) **50**, 9025-9030.
- Bunker, G., "Systematic Errors in Fluorescence EXAFS". See [http://gbxafs.iit.edu/training/Self\\_Absorption-effects.pdf](http://gbxafs.iit.edu/training/Self_Absorption-effects.pdf) (1988)
- Lee, J.M., Sung, N.-E., Park, J.-K., Yoon, J.-G., Kim, J.-H., Choi, M.-H. & Lee, K.-B., J. Synchrotron Rad. (1998), **5**, 524-526.
- Lytle, F.W., Gregor, R.B., Sandstrom, D.R., Marques, E.C., Wang, Joe, Spiro, C.L., Huffman, G.P. & Huggins, F.E., Nucl. Inst. Meth. (1984) **226**, 542-548.
- Oyanagi, H., J. Synchrotron Rad. (1998), **5**, 48-53.
- Stern, E.A. & Heald, S.M., Rev. Sci. Instrum. (1979) **50**, 1579-1582.
- Troger, L., Arvanitis, D., Baberschke, K., Michaelis, H., Grimm, U. & Zschech, E. (1992). Phys. Rev. B, **46**, 3283-3289.

(Received 10 August 1998; accepted 14 January 1999)